Proceedings of the 3rd International
IEEE EMBS Conference on Neural Engineering
Kohala Coast, Hawaii, USA, May 2-5, 2007

Can dipole modelling be improved by removing muscular and ocular artifacts from ictal scalp EEG?

Hans Hallez, Maarten De Vos, Ronald Phlypo, Bart Vanrumste, Peter Van Hese,
Yves D'Asseler, Wim Van Paesschen, Sabine Van Huffel and Ignace Lemahieu

Abstract— **Muscle artifacts and eye movement artifacts distort the EEG and make EEG dipole source localization near the ictal onset of the seizure very difficult and unreliable. Recently, two algorithms to remove these artifacts have been developed and validated. In our study we want to investigate if the multiple dipole model can be used in ictal EEG source localization. Furthermore, we want to investigate whether the use of the dipole model returns better interpretable results when artifacts are suppressed. The EEG dipole source localization was done by using the RAP-MUSIC algorithm. We used the relative residual energy as a goodness of fit for the dipole model. We found that in the unfiltered EEG the relative residual energy was very high, indicating that EEG dipole source localization is heavely affected by the noise. By removing the artifacts, we obtain a lower relative residual energy, which suggests that the multiple dipole model becomes an adequate model for EEG dipole source localization during ictal period.**

I. INTRODUCTION

Epilepsy is a chronical disorder that affects the daily life of people suffering from it. An epileptic seizure is the clinical manifestation of epilepsy and goes together with abnormal electric activity in the brain. The activity stems from clusters of neuronal sources which depolarize and repolarize synchronously. An electro-encephalogram (EEG) records this activity in function of time and is a very valuable tool in the diagnosis of patients suffering from epilepsy. In the presurgical evaluation, the patients are considered for a surgical removal of the epileptogenic focus. Therefore, a correct decision on the location of the focus is of crucial importance. A way to mathematically estimate the sources is EEG dipole source localization.

During an epileptic seizure, a lot of artifacts distort the EEG. These artifacts originate mainly from muscle activity and eye movements during the seizure. They decrease the readebility by the neurologist and the reliability of the solution to the EEG source localization problem. Recently, a muscle artifact removal technique was developed [1]. The technique is based on the assumption that the muscle activity has a low autocorrelation and uses this to identify sources associated with muscle activity. Several techniques are already proposed to remove artifacts caused by eye movements. Recently, we also developed a automatic eye artifact removal method based on Spatially Constrained Independent Component Analysis (SCICA) [2].

In this study we want to evaluate if the activity during a seizure can be modeled by a multiple dipole model. Furthermore, we want to investigate if the removal of the muscle and eye movement artifacts can improve the goodness of fit by a multiple dipole model during seizure activity. We can do this by observing the relative residual energy (RRE).

H. Hallez, P. Van Hese, R. Phlypo, Y. D'Asseler, I. Lemahieu are with Faculty of Engineering, Department of Electronics and Information Systems (ELIS), Medical Image and Signal Processing Group (MEDISIP), Ghent University, 9000 Ghent, Belgium hans.hallez@ugent.be

M. De Vos, B. Vanrumste and S. Van Huffel are with the Department of Electrical Engineering (ESAT), KU Leuven, 3000 Leuven, Belgium maarten.devos@esat.kuleuven.be

B. Vanrumste is also with the Katholieke Hogeschool Kempen, 2440 Geel, Belgium

W. Van Paesschen is with the Department of Neurology, Universitary Hospital Gasthuisberg, 3000 Leuven, Belgium

II. MATERIALS

The data sets were recorded in a clinical environment at the Gasthuisberg Universitary Hospital. A total of nine patients were considered. Each data set containes the start of a seizure and was checked by a physician upon a focal onset zone. The data was sampled at 250 Hz and measured using the standard 10-20 system, with a total of 21 electrodes.

III. METHODS

A. Removal of artifacts by Blind Source Separation (BSS) techniques

1) BSS techniques: BSS techniques recover a set of unknown source signals $\mathbf{S}(t) = [\mathbf{s}_1(t), ..., \mathbf{s}_K(t)]^T$ and $\mathbf{S} \in \Re^{K \times N}$, which are linearly mixed, with $t = 1, ..., N$, N the number of samples and K the number of sensors. The signals at the sensors $\mathbf{X}(t) = [\mathbf{x}_1(t), ..., \mathbf{x}_K(t)]^T$, $\mathbf{X} \in \Re^{K \times N}$ are the only available information and can be written as:

$$\mathbf{X}(t) = \mathbf{A} \cdot \mathbf{S}(t), \tag{1}$$

with $\mathbf{A} \in \Re^{K \times K}$ the unknown mixing matrix. When the mixing matrix is known, the source signals $\mathbf{S}(t)$ can be estimated, up to scaling and permutation indeterminateness, as

$$\mathbf{Z}(t) = a \cdot \mathbf{P} \cdot \mathbf{W} \cdot \mathbf{X}(t) \tag{2}$$

with $\mathbf{W}$ the de-mixing matrix, $\mathbf{P}$ is the permutation matrix and a is a scaling factor.

In general, it is only possible to estimate the mixing matrix when extra assumptions are made about the sources or the mixing matrix. This explains the variety of BSS algorithms that exist.

Artifacts can then be removed by setting the columns representing the activations of the artifactual sources equal

1-4244-0792-3/07/$20.00©2007 IEEE.

to zero in the reconstruction

$$\mathbf{X}_{clean}(t) = \mathbf{A}_{clean} \cdot \mathbf{Z}(t), \tag{3}$$

with $\mathbf{Z}(t)$ the sources obtained by BSS-CCA, and $\mathbf{A}_{clean}$ the mixing matrix with the columns in $\mathbf{A}$ representing activations of the artifactual sources, set to zero.

2) Muscle artifact removal by BSS-CCA: BSS-CCA is a blind source separation technique based on canonical correlation analysis, which assumes mutually uncorrelated sources which are maximally autocorrelated. BSS-CCA impose the previously mentioned constraints by using CCA with input $\mathbf{X}(t)$, the observed time courses and input $\mathbf{Y}(t)$, a temporally delayed version of the original data matrix ($\mathbf{Y}(t) = \mathbf{X}(t-1)$). Consider the linear combinations of the mean corrected components in $\mathbf{X}$ and $\mathbf{Y}$:

$$\begin{array}{l} \mathbf{u} = w_{x_1}\mathbf{x}_1 + ... + w_{x_K}\mathbf{x}_K = {\mathbf{w_x}}^T\mathbf{X}, \\ \mathbf{v} = w_{y_1}\mathbf{y}_1 + ... + w_{y_K}\mathbf{y}_K = {\mathbf{w_y}}^T\mathbf{Y}, \end{array} \tag{4}$$

CCA finds the weight vectors $\mathbf{w_x} = [w_{x_1}, ..., w_{x_K}]^T$ and $\mathbf{w_y} = [w_{y_1}, ..., w_{y_K}]^T$ that maximize the correlation ρ between the variates $\mathbf{u}$ and $\mathbf{v}$ [1], [3]. When CCA is used for blind source separation, as presented here, the variates $\mathbf{u}$ correspond to the sources and ρ to their autocorrelation [1]. Due to the broad frequency spectrum of EMG contamination in scalp EEG recordings, muscle artifacts resemble rather temporally white noise, which has a low autocorrelation. By consequence, the muscle artifact sources, or components, are always those with the lowest auto-correlation and can be removed [1].

3) Eye artifact removal by SCICA: The main disadvantage of ICA techniques is that the extracted sources are not ordered. Hence, all the sources need to be inspected to identify and extract the ones containing artifacts. However, in the case of eye artifacts, there is prior knowledge about the spatial potential distribution of these artifacts, as the position of the eyes does not change with respect to the electrodes. This prior knowledge can be used to constrain one (or more) sources during the ICA computation [4].

When the sources are individually correlated in time, but mutually uncorrelated, an ICA algorithm based on second order statistics can be derived: SOBI [5]. It is important to notice that extracting individually correlated signals with SOBI is different from extracting maximally autocorrelated signals with BSS-CCA. SOBI diagonalizes simultaneously a set of correlation matrices at different time lags. The solution of this simultaneous diagonalisation by plane rotations can be analytically computed by means of an iteration of Jacobi rotations. In SCICA, the cost function of these Jacobi rotations is changed in order to impose that the mixing vector of the last estimated source is similar to the known topography of the eye artifact.

After detection of eye artifacts, a 1.5 second epoch of EEG is used as input to SCICA in order to separate eye artifacts from other brain activity and remove them from the EEG [2].

B. EEG dipole source localization by RAP-MUSIC

When the muscle and eye artifacts are removed, one can search for the dipole sources. The EEG dipole localisation problem is twofold. First, the forward problem calculates the potential values at the scalp electrodes. This is done by solving Poisson's equation given a dipole source in a specified geometry. The head model we used, was a realistic head model derived from an T1 Magnetic Resonance scan. The head model was segmented in 4 compartments: scalp tissue, skull, cerebrospinal fluid (CSF) and brain tissue. The head model was then placed into a cubic calculation grid, where the internode distance was 1 mm. The conductivities of the compartments were isotropic and were equal 0.33 S/m, 0.020 S/m, 1 S/m and 0.33 S/m for scalp tissue, skull, CSF and brain tissue respectively. The 21 electrode positions were set in a standard 10-20 system. The forward problem was then solved by using a finite difference method [6].

Second, the inverse problem searches parameters of the dipole given the scalp potentials. A number of methods have been developed to estimate the dipolar source, depending on the assumptions of the input EEG potentials. In this study we used a multidipolar estimation technique, i.e. RAP-MUSIC [7].

The RAP-MUSIC algorithm uses the separation of the M-dimensional measurement space $\mathbf{V}$ into a signal Φ_{sig} and noise Φ_n subspace [7]. Consider a spatio-temporal model for the measurement data with additive white noise, $\mathbf{V} = \mathbf{AS} + \mathbf{N}$. The spatial autocorrelation matrix and it's Singular Value Decomposition (SVD) can be written as follows:

$$\begin{aligned} \mathbf{R}_v &= E\left\{\mathbf{V}(t)\mathbf{V}(t)^T\right\}, \\ &= [\mathbf{\Phi}_{sig}\mathbf{\Phi}_n] \begin{bmatrix} \mathbf{\Lambda}_{sig} & 0 \\ 0 & \mathbf{\Lambda}_n \end{bmatrix} [\mathbf{\Phi}_{sig}\mathbf{\Phi_n}]^T \end{aligned} \tag{5}$$

where $\mathbf{\Lambda}_{sig}$ and $\mathbf{\Lambda}_n$ are diagonal matrices with the singular values of $\mathbf{V}$ associated with the signal and noise subspace, resp.

The RAP-MUSIC consists of a exhaustive search of p sources, where the scalp potentials (calcaluted by the forward problem) have the highest subspace correlation with the signal subspace. The search algorithm scans through all possible source configurations looking for p peaks in the subspace correlation with the signal subspace. Errors in the estimation of Φ_{sig} reduce subspace correlation in a single global maximum and at $p-1$ local maxima. RAP-MUSIC avoids the problem of peak-picking by deflating the subspace spanned by the first source, which is found by taking the source with maximum subspace correlation. In this way the problem of finding 1 global maximum and $p-1$ local maxima is transformed into sequentially searching for p global maxima.

The relative residual energy is then defined as the relative amount of energy in the EEG that cannot be explained by the p dipoles, found by the RAP-MUSIC:

$$RRE = \frac{\|(\sum_i^p \mathbf{G}(\mathbf{r}_i, \mathbf{d_i})) - \mathbf{V}\|}{\|\mathbf{V}\|} \tag{6}$$

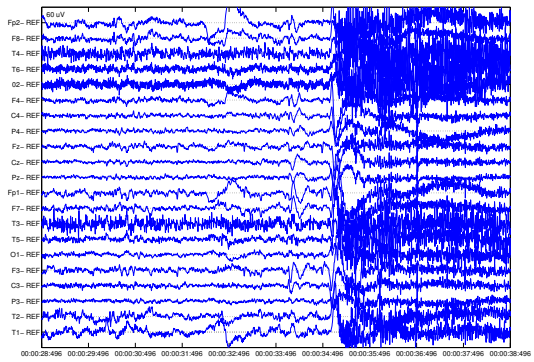

(a) unfiltered

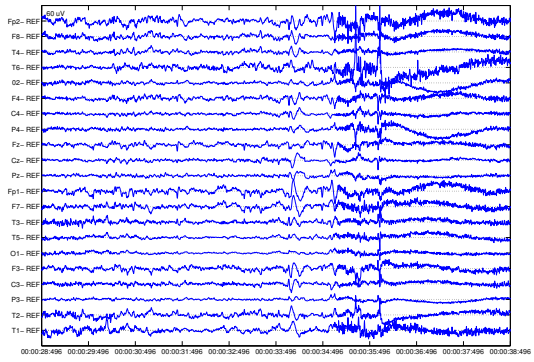

(b) filtered

Fig. 1. An 10 seconds example of (a) an unfiltered EEG and (b) a filtered EEG. The Y axis denote the different channels that are plotted and the X axis is the time frame. We can see that the muscle artifact on the channels 'T4', 'T6', 'O2' and 'T3' and the eye movement artifacts at 32-33 seconds has been removed by the artifact removal techniques.

where $\mathbf{G}(\mathbf{r}_i, \mathbf{d}_i)$ are the scalp potentials caused by the i-th dipole, calculated by solving the forward problem.

C. Data sets and simulation setup

The data was subjected to the artifact removal techniques, described above. For each patient we obtained an unfiltered and a filtered data set. On these data sets, the RAP-MUSIC algorithm was applied in moving windows of 128 samples (approximately 0.5 seconds at 250 Hz) and with steps of 16 samples. The signal subspace was formed from the highest energy components that had a total energy of 90%. The number of dipoles that are estimated was maximum 3, unless the correlation between the topography of the scanned source and the signal subspace was below 0.95, in which case the source is not taken into account and further scanning is stopped. The relative residual energy is then calculated according to equation 6 for each window.

The histogram of the RRE-values obtained by one data set is then used for evaluation. A probability density function was also fitted onto the histogram.

IV. RESULTS

Figure 1 shows an example of a filtered and an unfiltered EEG. The EEG's are plotted in a referential plot and the seizure start was at 33 seconds. We can see that the muscle artifact on the channels 'T4', 'T6', 'O2' and 'T3' and the eye movement artifacts at 32-33 seconds have been removed by the artifact removal techniques.

Figures 2 and 3 depict two typical results. Figure 2 shows the histograms and the estimated probability density function of the relative residual energy before and after the muscle artifact and eye movement artifact removal. Figure 2 shows a case where a high peak of low RRE-values was found after the artifact removal. Figure 3 is an example of a another patient. Here, the distribution of the RRE-values was shifted to the left. We see that the RRE-values are smaller. In seven of the nine cases the distribution of the RRE-values is shifted towards zero. One of the remaining cases is shown in figure 4. In these cases the distribution did not change, if the muscle artifact and eye movement artifact were removed. These cases did not have much muscle or eye movement artifacts present in the EEG.

V. CONCLUSIONS AND FUTURE WORKS

We use the relative residual energy as a goodness of fit the multidipolar source model for ictal EEG activity. We can appreciate from figures 2 and 3 that if we remove the muscle artifacts and eye artifact, the dipole sources become more adequate to model the EEG during a seizure. This indicates that the aforementioned muscle and eye artifact removal techniques can be used to improve the EEG dipole source localization. Future work will involve a validation of the found source with a golden standard. As a golden standard, this can be an ictal spect image.

REFERENCES

[1] W. De Clercq, A. Vergult, B. Vanrumste, W. Van Paesschen and S. Van Huffel, "Canonical correlation analysis applied to remove muscle artifacts from the electroencephalogram.", *IEEE Trans. Bio-Med. Eng.*, Vol. 53, pp. 2583-7, 2006

[2] M. De Vos, L. De Lathauwer, A. Vergult, W. De Clercq, W. Van Paesschen, S. Van Huffel. Spatially constrained independent component analysis algorithm for real-time eye artifact removal from the electroencephalogram. *Proc. of the first Annual Symposium of the IEEE-EMBS Benelux Chapter*. Brussels, Belgium, pp. 159-163 (2006)

[3] M. Borga and H. Knutsson. A Canonical Correlation Approach to Blind Source Separation. Report LiU-IMT-EX-0062 Department of Biomedical Engineering, Linkping University, 2001

[4] L. Shoker, S. Sanei, W. Wang, J.A. Chambers. Removal of eye blinking artifact from the electro-encephalogram, incorporating a new constrained blind source separation algorithm. *Med Biol Eng Comput*, 43, 290-295, 2005

[5] A. Belouchrani, K. Abed-Meraim, J.-F. Cardoso, and E. Moulines. A blind source separation technique using second order statistics. *IEEE Trans. Signal Processing*, 45, pp. 434444, 1997.

[6] H. Hallez, B. Vanrumste, P. Van Hese, Y. D'Asseler, I. Lemahieu and R. Van de Walle, "A Finite Difference Method with Reciprocity used to Incorporate Anisotropy in electroencephalogram dipole source localization", *Physics in Medicine and Biology*, Vol. 50, pp. 3787-3806, 2005

[7] J.C. Mosher and R.M. Leahy, "Source Localization Using Recursively Applied and Projected (RAP) MUSIC", *IEEE Transactions on Signal Processing*, Vol. 47, pp. 332-340, 1999

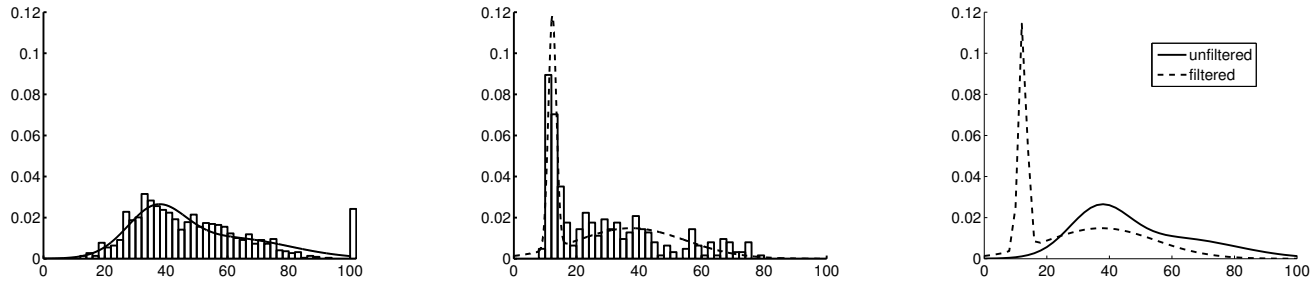

(a) unfiltered (b) filtered (c) comparison

Fig. 2. The histograms and the estimated probability density function the RRE-values of a first patient. The X-axis of figure (a), (b) and (c) denote the relative residual energy, the Y-axis shows the probability that an RRE value occurs. The solid line shows the distibution of the RRE-values using the unfiltered EEG and the dashed line shows the distribution when the EEG has been filtered. Figure (a) and (b) shows the histogram and the pdf in the unfiltered and filtered case, respectively. Figure (c) shows a figure where the pdf's of filtered and unfiltered are plotted together.

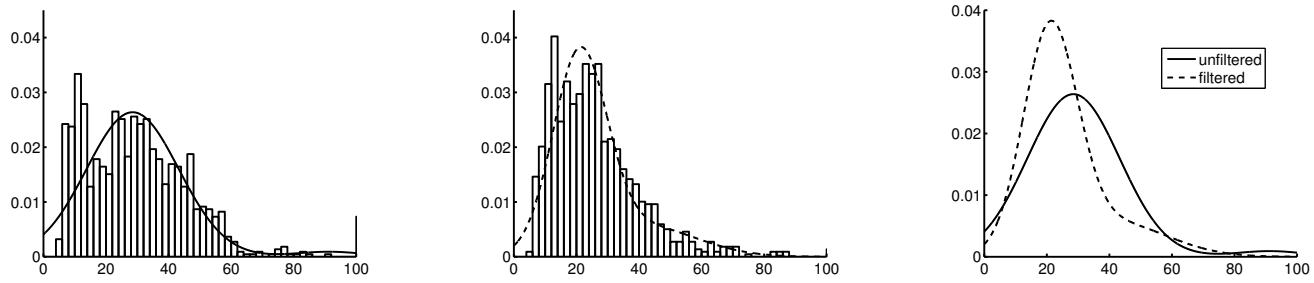

(a) unfiltered (b) filtered (c) comparison

Fig. 3. The histograms and the estimated probability density function the RRE-values of a second patient. The X-axis of figure (a), (b) and (c) denote the relative residual energy, the Y-axis shows the probability that an RRE value occurs. The solid line shows the distibution of the RRE-values using the unfiltered EEG and the dashed line shows the distribution when the EEG has been filtered. Figure (a) and (b) shows the histogram and the pdf in the unfiltered and filtered case, respectively. Figure (c) shows a figure where the pdf's of filtered and unfiltered are plotted together.

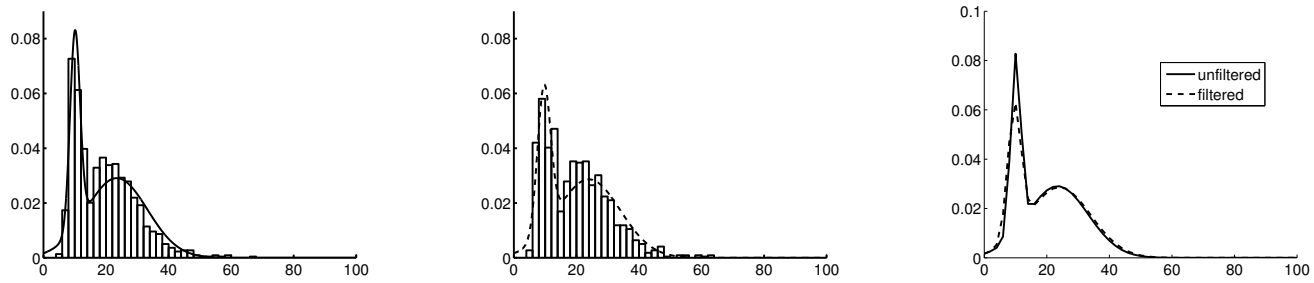

(a) unfiltered (b) filtered (c) comparison

Fig. 4. The histograms of the fitted distribution of the RRE-values, when the artifact removal resulted in the same distribution as the unfiltered EEG. The X-axis of figure (a) and (b) denote the relative residual energy, the Y-axis shows the probability that an RRE value occurs. The solid line shows the distibution of the RRE-values using the unfiltered EEG and the dashed line shows the distribution when the EEG has been filtered. Figure (a) shows a case where the after the artifact removal a high peak of low RRE-values were found. Figure (b) shows a figure where the distribution of the RRE-values were shifted to the left.